2006gl026923-txts01.tex

Contains The description of the numerical model used in our study:

Modeling the oxygen-isotopic composition of the North American Ice Sheet and its effect on the isotopic composition of the ocean during the last glacial cycle

Adriana Sima

Department of Geosciences, University of Bremen, Bremen, Germany.

Now at Institut des Sciences de l'Evolution, Universite Montpellier II, Montpellier, France

André Paul and Michael Schulz

Department of Geosciences and Research Center Ocean Margins, University of Bremen, Bremen, Germany

Johannes Oerlemans

Institute for Marine and Atmospheric research Utrecht, Utrecht University, Utrecht, Netherlands

We constructed a 2.5-dimensional thermomechanical ice-sheet model by combining the computation along a north-south flow line after *Payne* [1995] with an equilibrium profile in the zonal direction following *Gallée et al.* [1992] and *Crucifix and Berger* [2002]. Our model simulates the North-American Ice Sheet (NAIS), which dominated ice-volume variations during the late Pleistocene.

Ice-Sheet Model

The ice-surface elevation is denoted by $s = H + h$, where H is the ice thickness and h the bedrock elevation with respect to present-day sea level.

The evolution of ice-sheet thickness at the divide as a function of latitude φ is given by the continuity equation [cf. *Gallée et al.*, 1992, equation 1 therein]:

$$\frac{\partial H}{\partial t} = M - \frac{1}{a\cos\varphi}\frac{\partial}{\partial\varphi}\left(\overline{u_y}H\cos\varphi\right) - D_\lambda - S, \tag{1}$$

where M is the local annual mass balance at ice surface, a the radius of the Earth, $\bar{u}$ is the vertically-averaged horizontal velocity, D_λ represents the lateral discharge of ice mass and S the melt rate at the ice-sheet base (see Table 1 for parameter values).

In the east-west direction, a perfectly-plastic profile symmetric to the ice-sheet crest is assumed [*Gallée et al.*, 1992; *Crucifix and Berger*, 2002]. For the zonal ice-mass discharge we employ a parameterization similar to *Gallée et al.* [1992]:

$$D_\lambda = -\frac{1}{(a\cos\varphi)^2}DH\frac{\partial^2 s}{\partial\lambda^2} = DH\frac{s}{L^2} \tag{2}$$

with $D = 8\bar{A}\frac{(\rho g)^n}{a^2}\left|\frac{\partial s}{\partial\varphi}\right|^{n-1}$, where $\bar{A}$ is the vertically integrated (in our case temperature-dependent) flow parameter and L is the longitudinal extent of the ice sheet. The parameter L is related to the ice surface elevation as follows:

$$L = s^2/\mu \tag{3}$$

with $\mu = \frac{2\tau_0}{\rho g}$, where r is the ice density, g the gravitational acceleration and τ_0 the prescribed, constant bottom stress, derived from the *CLIMAP* [1981] reconstruction [*Crucifix and Berger*, 2002].

A vertical distribution of the lateral discharge, consistent with the perfect-plasticity assumption, is:

$$d_\lambda(z) = \frac{1}{H}D_\lambda, \tag{4}$$

with $\int_h^s d_\lambda(z)dz = D_\lambda$.

In the north-south direction ice deformation is assumed to be driven by horizontal shear stress (τ_{yz}), approximated by:

$$\tau_{yz}(z) = -\rho g(s-z)\frac{\partial s}{\partial y}. \tag{5}$$

Assuming a nonlinear Glen flow law for ice, the meridional velocity is derived as:

$$u_y(z) = -2\frac{(\rho g)^n}{a^2}\left|\frac{\partial s}{\partial \varphi}\right|^{n-1}\frac{1}{a}\frac{\partial s}{\partial \varphi}\int_h^z A(T^*)(s-z)^n dz + u_y(h), \tag{6}$$

where $u_y(h)$ is the meridional component of the sliding velocity.

The parameter A introduces the temperature dependence of ice deformation. It is assumed to be an Arrhenius-type function of the absolute temperature of the ice, corrected for the dependence of the melting point on pressure (T^*):

$$A(T^*) = EA_0 \exp\left(\frac{-Q}{RT^*}\right), \tag{7}$$

with:

$$T^* = T - T_{pmp} + T_0, \tag{8}$$

$$T_{pmp} = T_0 - \rho_i g \Phi(s-z), \tag{9}$$

where T is ice temperature, T_{pmp} the pressure melting point temperature, T_0 the triple point temperature of water and Φ the rate of change of melting point temperature with pressure.

Furthermore, in eq.(7), Q is the creep activation energy, R is the universal gas constant, A_0 is a constant coefficient and E an empirical flow enhancement factor introduced into Glen's flow law to account for the effects of crystal anisotropy and impurities on bulk ice deformation [*Marshall et al.*, 2000]. The values for A_0 and Q are those indicated in the EISMINT II model intercomparison project [*Payne et al.*, 2000].

The vertically integrated flow coefficient used in the calculation of lateral discharge is obtained by numerically integrating $\bar{A} = \int_h^s \left(\int_h^z A(T^*)(s-z')^n dz'\right) dz$.

The sliding velocity is assumed to be directly related to basal shear stress:

$$\begin{cases} u_y(h) = -B\rho g H \frac{\partial s}{\partial y} & \text{if } T_{base} = T_{pmp} \\ u_y(h) = 0 & \text{if } T_{base} < T_{pmp} \end{cases} \tag{10}$$

where T_{base} is the basal ice temperature and B a free parameter. A numerical integration of equation (6) provides the vertically averaged horizontal velocity employed in (1).

The distribution of vertical velocity can be found from the meridional velocities calculated in (6) and the lateral discharge profile (4), using the incompressibility condition:

$$w(z) = -\int_h^z \frac{\partial u_y}{\partial y} dz - \int_h^z d_\lambda dz + w(h), \tag{11}$$

with the velocity at ice-sheet base:

$$w(h) = \frac{\partial h}{\partial t} + u_y(h)\frac{\partial h}{\partial y} - S, \tag{12}$$

where S is the basal melt rate.

Bedrock adjustment is computed from a local lithosphere–relaxed asthenosphere model [*Le Meur and Huybrechts*, 1996] with a characteristic time constant τ_b :

$$\frac{\partial h}{\partial t} = \frac{1}{\tau_b}\left[h_{eq} - h - \frac{\rho H}{\rho_b}\right], \tag{13}$$

where h_{eq} is the equilibrium bedrock elevation with respect to present-day sea level and ρ_b the bedrock density. The initial topography along the flow line is taken from *Clark and Pollard* [1998]: 500 m above sea level southward of 70N, -500 m northward of 74N and a linear ramp between 70 and 74N.

The ice temperature T influences the model dynamics in two ways: it determines the flow parameter A used in computing horizontal velocity and lateral discharge, and it determines whether or not sliding occurs. The equation for temperature evolution contains vertical diffusion, horizontal and vertical advection and frictional heat generation terms:

$$\frac{\partial T}{\partial t} = \frac{k}{\rho c}\frac{\partial^2 T}{\partial z^2} - u_y\frac{\partial T}{\partial y} - d_\lambda T - w\frac{\partial T}{\partial z} + \frac{\tau_{yz}}{\rho c}\frac{\partial u_y}{\partial z}, \tag{14}$$

where k is ice thermal conductivity and c ice specific heat capacity.

When the temperature computed for the basal layer (T_{base}) exceeds the pressure melting point, a melt rate is calculated:

$$S = \frac{c}{\lambda}\left(T_{base} - T_{pmp}\right)\frac{\Delta z_{base}}{\Delta t}, \tag{15}$$

where λ is the latent heat capacity of ice, Δz_{base} the thickness of the basal layer, and Δt the timestep (see section “Numerical Solution“ for details of the discretization). After computing the melt rate, T_{base} is reset to T_{pmp}.

Enhanced flow in the zonal direction during periods when the basal temperature is at the melting point is represented by a gradual decrease of the bottom stress τ_0 with a rate $d\tau/dt = 0.2$ Pa/yr. This parameterization is based on the treatment of Heinrich events by *Crucifix and Berger* [2002] and results in increasing the lateral discharge by an additional term [cf. *Crucifix and Berger*, 2002, Appendix B therein]:

$$\frac{\partial s}{\partial t} = -\frac{1}{\tau}\frac{d\tau}{dt}\frac{s^2 - sh}{3s - 2h} \tag{16}$$

The decrease of τ_0 is limited to a minimum value of 10,000 Pa.

Ice-volume computation also follows *Crucifix and Berger* [2002, Appendix A therein]. The volume of an ice-sheet slice comprised in a latitude band of width $\Delta\varphi$ is:

$$V_{\Delta\varphi} = \begin{cases} \frac{2}{3}\frac{2s^2(s-h)}{\mu} a\Delta\varphi & \text{if } \; 2L \leq x_p(\varphi) \\ \frac{4}{3}\left[L^{3/2} - \left(L - \frac{x_p}{2}\right)^{3/2}\right]\sqrt{\mu}\left(1 - \frac{h}{s}\right) a\Delta\varphi & \text{if } \; 2L > x_p(\varphi) \end{cases} \tag{17}$$

where $x_p(\varphi)$ is the width of the continental platform [cf. Crucifix and Berger, 2002, Figure 1a therein].

Tracer Treatment

The ratio R of oxygen isotopes ^{18}O and ^{16}O is expressed as the fractional deviation from the isotopic ratio of the Vienna Standard Mean Ocean Water [V-SMOW, *Gonfiantini*, 1978]:

$$\delta^{18}\text{O} = (R/R_{V-SMOW} - 1) \times 1000\% \tag{18}$$

Ice-δ^{18}O (δ for short) is introduced in the model as a passive tracer. There is no diffusion for δ and its transport through ice relies on the same advection scheme (first-order upwind) as temperature:

$$\frac{\partial \delta}{\partial t} = -u_y\frac{\partial \delta}{\partial y} - d_\lambda \delta - w\frac{\partial \delta}{\partial z}, \tag{19}$$

Using δ directly rather than mass ratio introduces a negligible conservation error.

By equation (19), the model only computes the two-dimensional distribution of δ along the flow line, as it does for temperature by equation (14). In order to derive the mean isotopic composition of the whole ice sheet (δ_i), knowledge on the isotopic distribution in the East-West direction would be required. As snow falling at the ice-sheet crest has the longest residence time in the ice, the solution we choose is to approximate δ_i by the mean computed along the flow line:

$$\delta_i \equiv \frac{\int_{\varphi_S}^{\varphi_N}\int_0^{H(\varphi)} \delta(\varphi, z)\, dz d\varphi}{\int_{\varphi_S}^{\varphi_N} H(\varphi)\, d\varphi} \tag{20}$$

where φ_N and φ_S are the latitudes of the northern and, respectively, southern margins of the ice sheet.

We note that equation (20) contains no weighting by the width, or the area of the latitudinal (parabolic) profile, or by a function of them. Such weighting would imply ad-hoc assumptions on the isotopic distribution perpendicular to the flow line, and we prefer to avoid that.

As the ice at the divide is the most depleted, our approach is likely to result in an underestimation (in the sense of a more negative value) of the mean δ^{18}O of the ice sheet (δ_i). No weighting also implies that the relative contribution of the isotopically heavier ice from southern latitudes (where the ice-sheet is thinner) to the mean is increased in comparison to a weighting approach, which may attenuate the underestimation of δ_i .

Numerical Solution

The glacial cycle integration extends from 120 kyr BP to the present. We use an Eulerian-forward scheme for time stepping. The timestep is 1 year, except for periods of intense melting at the ice-sheet base or high ablation at ice surface, when it is reduced to 0.05 year. Staggered grids are employed in both horizontal and vertical directions. The latitudinal-grid resolution is 0.5. The vertical grid is stretched and has 12 uneven layers, with thicknesses decreasing towards the ice-sheet base.

We use a first-order upwind scheme for advection and a second-order scheme for heat diffusion. Vertical upwinding is done using the relative vertical velocity ($w*$), i.e., the difference between the vertical velocity of the ice and that of the grid point [*Payne and Dongelmans*, 1997, Appendix A therein]. At the ice surface $w^*_{sfc} = -M$, and at the base $w^*_{base} = -S$.

Boundary Conditions

Flux boundary conditions are applied at the ice-sheet surface and base.

The advective heat fluxes are:

$$F^T_{sfc} = \begin{cases} \rho c M T_a & \text{if } M \geq 0 \\ \rho c M T_{sfc} & \text{if } M < 0 \end{cases} \tag{21}$$

at the ice surface, where T_a is the air temperature at ice surface and T_{sfc} the temperature of the upper ice layer, and

$$F^T_{base} = -\rho c S T_{base} \tag{22}$$

at ice-sheet base.

The advective fluxes for δ^{18}O are:

$$F_{sfc}^{\delta} = \begin{cases} M\delta_{snow} & \text{if } M \geq 0 \\ M\delta_{sfc} & \text{if } M < 0 \end{cases}, \tag{23}$$

and

$$F_{base}^{\delta} = -S\delta_{base}, \tag{24}$$

where δ_s denotes the isotopic composition of snow, δ_{sfc} is the δ^{18}O of the upper ice layer and δ_{base} the δ^{18}O of the bottom layer.

The diffusive heat fluxes are:

$$\begin{cases} Q_{sfc}^{T} = \rho c \Delta z_{sfc} \left(T_a - T_{sfc}\right) / \tau_{damp} \\ Q_{base}^{T} = -G \end{cases}, \tag{25}$$

where Δz_{sfc} is the thickness of the uppermost ice layer, τ_{damp} the time scale for restoring the surface temperature T_{sfc} to the prescribed air temperature T_a, and G the geothermal heat flux.

The diffusive fluxes for δ^{18}O are nul.

Climate Forcing

The local annual mass balance M on the ice surface is derived using the equilibrium-line concept, as follows [*Oerlemans*, 1982]:

$$M = \min\left[M_{\max}, M_{\max}\left(s - h_{equ}\right)/h_{\max}\right] \quad \text{m yr}^{-1} \tag{26}$$

where the upper limit for the accumulation rate M_{max} and the parameter h_{max} are similar to those used by *Pollard* [1983].

The equilibrium-line elevation h_{equ} is computed as a function of near-surface air temperature T_a and elevation:

$$h_{equ} = s + \left(T_a - T_{equ}\right)/\beta \tag{27}$$

where β is the atmospheric lapse rate, and T_{equ} the equilibrium-line temperature [*Oerlemans*, 1982].

The near-surface air temperature parameterization follows the glacial index method of *Marshall et al.* [2000]:

$$\begin{aligned} T_a(\varphi, t) &= T(\varphi, 0) + I(t)[T(\varphi, 21) - T(\varphi, 0)] \\ &-\beta\{s(\varphi, t) - s(\varphi, 0) - I(t)[s(\varphi, 21) - s(\varphi, 0)]\} \end{aligned} \tag{28}$$

where the glacial index $I(t)$ is derived from the NGRIP δ^{18}O record [*North Greenland Ice Core Project members*, 2004] by assigning climate indices of $I = 0$ to present-day and $I = 1$ to LGM d18O values in the ice core and linearly interpolating between these end members. Latitudinal distributions of surface temperature at present day, $T(\varphi, 0)$, and at LGM, $T(\varphi, 21)$, are computed by zonally averaging the output of the atmospheric general circulation model ECHAM3/T42 [*Romanova et al.*, 2004, Figure 1c therein] over the North-American continent.

The parameterization of the oxygen-isotopic composition of snow combines the relationship between mean annual surface temperature and δ^{18}O of precipitation derived by *Johnsen and White* [1989] for present-day Greenland, the results of AGCM simulations by *Jouzel et al.* [1994] and the glacial index:

$$\delta_s = -13.7 + \alpha(t) T_a \tag{29}$$

with the slope a(t) computed as:

$$\alpha(t) = \alpha_0 + I(t) \left[\alpha_{LGM} - \alpha_0\right] \tag{30}$$

where α_0 and α_{LGM} are the slopes determined by *Jouzel et al.* [1994] for the NAIS domain for present day and the LGM, respectively.

References

Clark, P.U., and D. Pollard (1998), Origin of the middle Pleistocene transition by ice sheet erosion of regolith, Paleoceanogr., 13 (1), 1-9.

CLIMAP Project members (1981), Seasonal reconstructions of the Earth's surface at the last glacial maximum, Geological Society of America.

Crucifix, M., and A. Berger (2002), Simulation of ocean-ice sheet interactions during the last deglaciation, Paleoceanogr., 17 (4), 1054, 10.1029/2001PA000702.

Gallée, H., J.P. van Ypersele, T. Fichefet, C. Tricot, and A. Berger (1992), Simulation of the last glacial cycle by a coupled, sectorially averaged climate-ice sheet model. Part II: Response to insolation and CO2 variations, J. Geophys. Res., 97, 15713-15740.

Gonfiantini, R. (1978), Standards for stable isotope measurements in natural compounds, Nature, 271, 534-536.

Johnsen, S.J., and J. White (1989), The origin of Arctic precipitation under present and glacial conditions, Tellus, 41B, 452-468.

Jouzel, J., R.D. Koster, R.J. Suozzo, and G.L. Russell (1994), Stable water isotope behavior during the last glacial maximum: A general circulation model analysis, J. Geophys. Res., 99 (D12), 25791-25801.

Le Meur, E., and P. Huybrechts (1996), A comparison of different ways of dealing with isostasy: examples from modelling the Antarctic ice sheet during the last glacial cycle, Annal. Glaciol., 23, 309-317.

Marshall, S.J., L. Tarasov, G.K.C. Clarke, and W.R. Peltier (2000), Glaciological reconstruction of the Laurentide Ice Sheet: physical processes and modelling challenges, Can. J. Earth Sci., 37, 769-793.

North Greenland Ice Core Project members (2004), High-resolution record of Northern Hemisphere climate extending into the last interglacial period, Nature, 431, 147-151.

Oerlemans, J. (1982), Glacial cycles and ice-sheet modelling, Clim. Change, 4, 353-374.

Payne, A.J. (1995), Limit cycles in the basal thermal regime of ice sheets, J. Geophys. Res., B100, 4249-4263.

Payne, A.J., and P.W. Dongelmans (1997), Self-organization in the thermomechanical flow of ice sheets, J. Geophys. Res., B102, 12219-12233.

Payne, A.J., P. Huybrechts, A. Abe-Ouchi, R. Calov, J.L. Fastook, R. Greve, S.J. Marshall, I. Marsiat, C. Ritz, L. Tarasov, and M.P.A. Thomassen (2000), Results from the EISMINT model intercomparison: the effects of thermomechanical coupling, J. Glaciol., 46 (153), 227-238.

Pollard, D. (1983), Ice-age simulations with a calving ice-sheet model, Quat. Res., 20, 30-48.

Romanova, V., M. Prange, and G. Lohmann (2004), Stability of the thermohaline circulation and its dependence on the background hydrological cycle, Clim. Dyn., 22, 527-538.

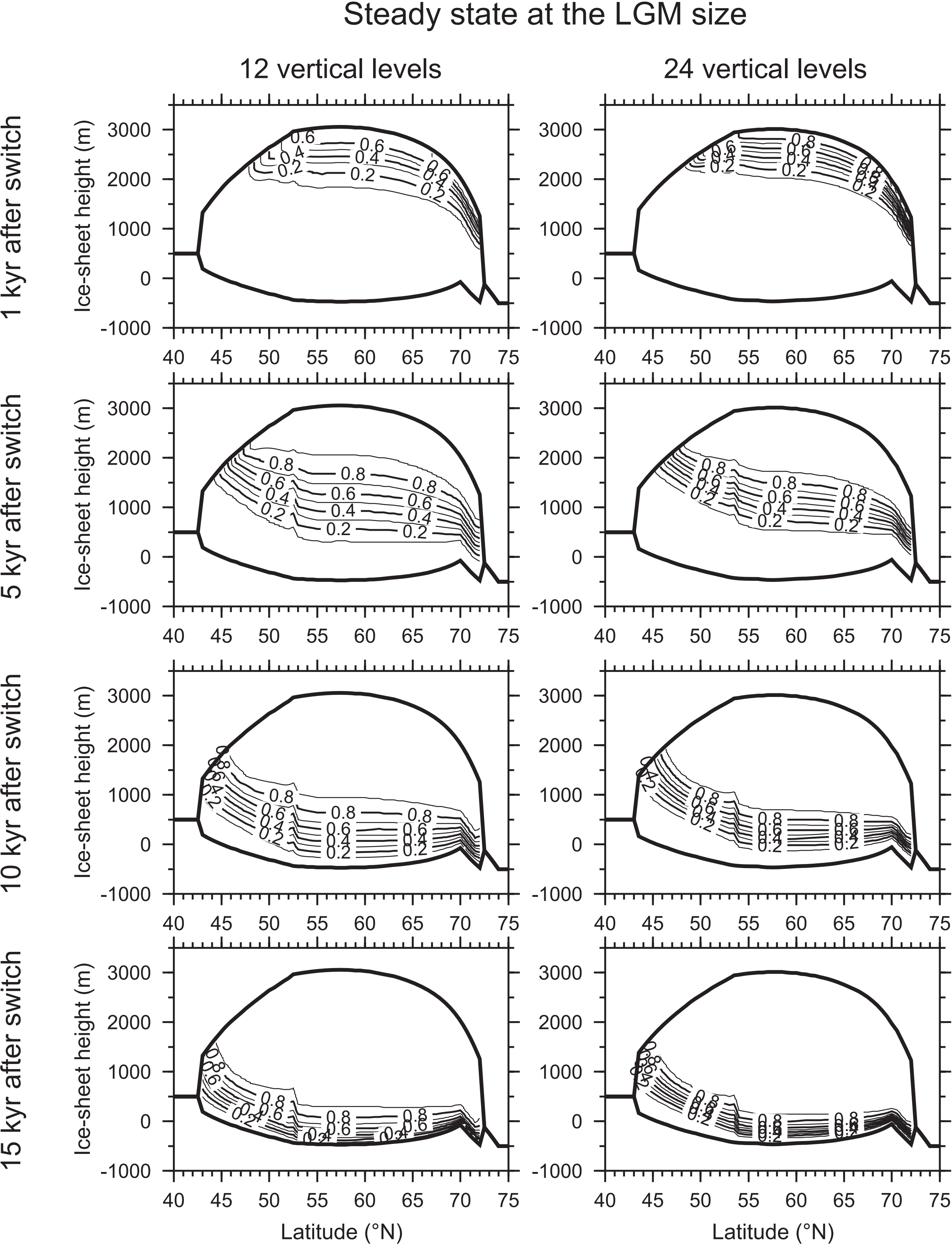
Steady state at the LGM size
12 vertical levels
24 vertical levels
1 kyr after switch
5 kyr after switch
10 kyr after switch
15 kyr after switch
Ice-sheet height (m)
Latitude (°N)

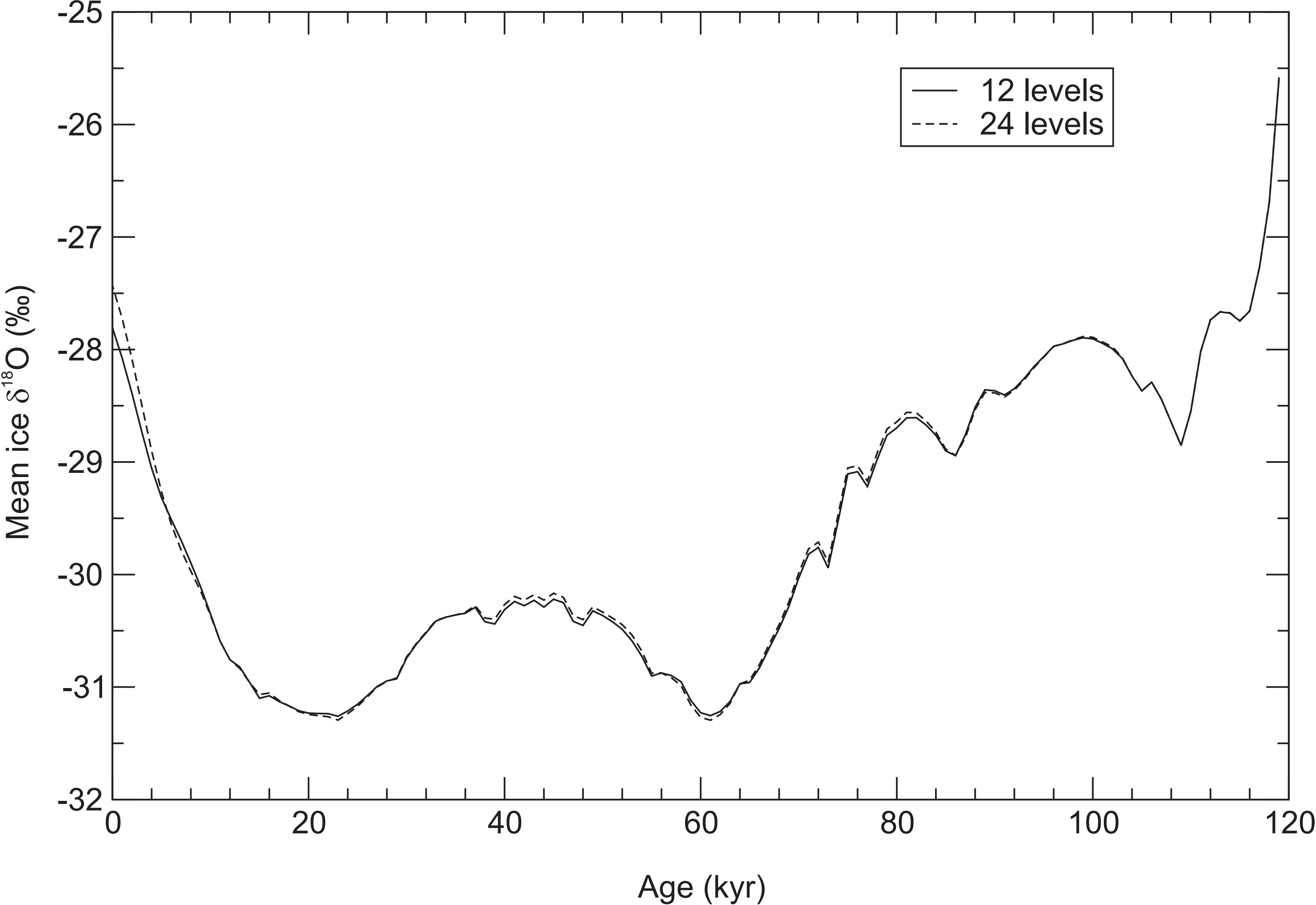

12 levels
24 levels
Mean ice δ18O (‰)
-25
-26
-27
-28
-29
-30
-31
-32
0
20
40
60
80
100
120
Age (kyr)